



1 **How size and trigger matter: analyzing rainfall- and earthquake-triggered landslide inventories** 2 **and their causal relation in the Koshi River basin, Central Himalaya**

3
4 Jianqiang Zhang ^{1,2}, Cees J. van Westen ², Hakan Tanyas ², Olga Mavrouli ², Yonggang Ge ¹, Samjwal Bajrachary ³,
5 Deo Raj Gurung ³, Megh Raj Dhital ⁴, Narendral Raj Khanal ⁵

6 ¹Key Laboratory of Mountain Hazards and Surface Process/Institute of Mountain Hazards and Environment, Chinese Academy of
7 Sciences, Chengdu, China.

8 ²Faculty of Geo-Information Science and Earth Observation (ITC), University of Twente, the Netherlands.

9 ³International Centre for Integrated Mountain Development (ICIMOD), Lalitpur, Nepal.

10 ⁴The Department of Geology, Tri-Chandra Multiple Campus, Ghantaghar, Kathmandu, Nepal.

11 ⁵Central Department of Geography, Tribhuvan University, Kathmandu, Nepal.

12 *Correspondence to:* Jianqiang Zhang(zhangjq@imde.ac.cn)

13
14 **Abstract:** Inventories of landslides caused by different triggering mechanisms, such as earthquakes, extreme rainfall
15 events or anthropogenic activities, may show different characteristics in terms of distribution, causal factors and
16 frequency-area relationships. The aim of this research is to study such differences in landslide inventories, and the
17 effect they have on landslide susceptibility assessment. The study area is the watershed of the trans-boundary Koshi
18 River in central Himalaya, shared by China, Nepal and India. Detailed landslide inventories were generated based on
19 visual interpretation of remote sensing images and field investigation for different time periods and triggering
20 mechanisms. Maps and images from the period 1992 to 2015 were used to map 5,858 rainfall-triggered landslides and
21 after the 2015 Gorkha earthquake, an additional 1138 co-seismic landslides were mapped. A set of topographic,
22 geological and land cover factors were employed to analyze their correlation with different types and sizes of
23 landslides. The results show that the frequency - area distributions of rainfall and earthquake-triggered landslides
24 varied considerably, with the former one having a larger frequency of small landslides. Also topographic factors varied
25 considerably for the two triggering events, with both elevation and slope angle showing significantly different patterns
26 for earthquake-triggered and rainfall-triggered landslides. Landslides were classified into two size groups, in
27 combination with the main triggering mechanism (rainfall- or earthquake-triggered). Susceptibility maps for different
28 combinations of landslide size and triggering mechanism were generated using logistic regression analysis. The
29 different triggers and sizes of landslide data were used to validate the models. The results showed that susceptible areas
30 for small and large size rainfall- and earthquake-triggered landslides differed substantially, while susceptibility maps
31 for different size of earthquake-triggered landslides were similar.

32
33 **Key words:** landslides, rainfall-triggered, earthquake-triggered, frequency-area analysis, susceptibility assessment,



34 Nepal

35

36 1. Introduction

37

38 Landslides are one of the most harmful geological hazards causing substantial fatalities and loss of property
39 worldwide, affecting settlements, agriculture, transportation infrastructure and engineering projects (Dilley et al. 2005;
40 Petley, 2012; Zhang et al., 2015; Haque et al., 2016). Among the various characteristics that determine the potential
41 damage of landslides, size plays an important role, as well as velocity, depth, impact pressure, or displacement which
42 differs for the various mass movement types. Volume may be an even more important landslide characteristic than size,
43 but this is difficult to measure as it requires specific geophysical or geotechnical methods that can be applied at a site
44 investigation level, or the use of multi-temporal Digital Elevation Models (SafeLand, 2015; Martha et al., 2017).
45 Therefore, empirical relations between landslide area and volume are generally used (Dai and Lee, 2001; Guzzetti et
46 al., 2008; Larsen et al., 2010; Klar et al., 2011; Larsen and Montgomery, 2012). To investigate whether earthquake- and
47 rainfall-triggered landslides inventories have similar area-frequency distributions, area-volume relations and spatially
48 controlling factors, it is important to collect event-based landslide inventories. The difficulty is to collect complete
49 inventories that are independent for earthquakes and rainfalls.

50 Many studies that compare the characteristics of earthquake- and rainfall-triggered landslide inventories focus on
51 mapping landslides triggered by rainfall after major earthquakes. For example, Lin et al. (2006) and Chang et al.
52 (2007) studied the difference between earthquake- and typhoon-triggered landslides in mountainous watersheds in
53 Taiwan. Landslides were mapped from eight satellite images covering a period between 1996 and 2001 and concluded
54 that the density of rainfall-triggered landslides increased significantly after the earthquake, and the places where
55 landslides occurred changed, and concluded that different triggers produced significantly different patterns, with
56 rainfall-triggered landslides occurring more near channels and earthquake-triggered ones close to ridges.

57 Menuier et al. (2008) compared rainfall-triggered landslides in the western Southern Alps of New Zealand with some earthquake-
58 triggered landslides, and found that the rainfall-triggered landslides were evenly distributed over all slope segments,
59 and the landslide susceptibility was lower near ridge crests. Tang et al. (2011) mapped landslides in the Beichuan area
60 after the 2008 Wenchuan earthquake in China. They mapped 2221 co-seismic landslides but also 696 rainfall-triggered
61 landslides which occurred several months later, and which were located in the same area, as most of them were
62 reactivations of the co-seismic landslides. Tang et al. (2016) analyzed changes in landslide activity near the epicenter
63 of the 2008 Wenchuan earthquake by generating five landslide inventories for different years through stereoscopic
64 digital visual image interpretation. From May 2008 to April 2015, 660 new landslides occurred outside the co-seismic
65 landslide areas. In April 2015, the number of active landslides had gone down to 66, less than 1% of the co-seismic



66 landslides, still much higher than the pre-earthquake situation. The problem with the studies indicated above is that
67 rainfall-triggered landslides that occur shortly after a major earthquake are generally following the same patterns, due
68 to the availability of large volumes of landslide materials of the co-seismic landslides. There are fewer studies that
69 compare the two triggering mechanisms in an independent manner.

70 Landslide susceptibility assessment is carried out to define the landslide-prone areas depending on potential causal
71 factors (or internal factors that make certain areas susceptible to landslides) and triggering factors (which are external
72 dynamic factors which initiate the landslide event). In medium and regional scale landslide susceptibility assessment,
73 statistical methods are commonly used (Carrara et al. 1995; Soeters and van Westen 1996; Chung and Fabbri 1999;
74 Guzzetti et al. 1999; Duman et al. 2006; Bathrellos et al. 2009). Causal factors generally include topographical factors
75 (slope gradient, elevation difference, slope aspect etc.), geological factors (lithology, joints, faults, etc.) and land use
76 factors (current land use, land use changes, slope cuts etc.) (Kamp et al. 2008). The spatial representation of dynamic
77 triggering factors is often complicated to analyze (e.g. topographic amplification and peak ground acceleration during
78 earthquakes or water tables during extreme rainfall events) because of the large uncertainty of soil depth and soil
79 conditions over certain areas. Therefore these triggering factors are often not included within landslide susceptibility
80 assessment. As historical evidence is a key input in the prediction of future landslide events, landslide inventories are
81 one of the most important inputs in statistical landslide susceptibility assessment. However, complete inventories are
82 scarce, and landslide inventories often reflect the results of the last triggering event (van Westen et al. 2008).

83 There is no clear evidence shows the difference on morphology between rainfall-triggered landslide and earthquake-
84 triggered landslide. But some statistics on landslides with causal factors show the difference induced by different
85 triggers. Fan et al. (2012) found that, when volume smaller than $10 \times 10^4 \text{m}^3$, both rainfall-triggered landslide and
86 earthquake-triggered landslide have similar distance of runout; when volume larger than $10 \times 10^4 \text{m}^3$, the earthquake-
87 triggered landslide has longer runout than rainfall-triggered landslide. Different size of landslide show different
88 characteristics. The large size landslides can generate high speed and long distance hazard due to the wide range of
89 instability area and huge potential energy. Korup et al. (2007) found that relative relief and rock strength are the
90 significant factors to affect the occurrence of large size landslides. Peng et al. (2014) analyzed the landslides in the
91 Three Gorges area and found that medium size and large size of earth slides are located in a wide range of elevation, as
92 well as large size rock slides; Most small size, large size and huge size of rock slides are located in north slopes;
93 medium and large size landslides mostly occur at shale, sandstone and mudstone and other soft stratum, as well as
94 carbonate rock and clastic rock interbedded stratum.

95 The first question that will be addressed in this research is whether it is possible to utilize inventories of earthquake-
96 triggered landslides (ETL) as inputs for analyzing the susceptibility of rainfall-triggered landslides (RTL). Although
97 landslide size is often considered important in hazard assessment and risk assessment, it is generally not considered as



98 a separate component of the susceptibility assessment. The second question that will be investigated in this study is
99 whether different landslide size groups are controlled by different sets of causal factors.

100 The aim of this study is to investigate the differences in the mappable characteristics of earthquake-triggered and
101 rainfall triggered landslides in terms of their frequency-area relationships, spatial distributions and relation with causal
102 factors, and to evaluate whether separate susceptibility maps generated for specific landslide size and triggering
103 mechanism are better than a generic landslide susceptibility assessment including all landslide sizes and triggers.

104

105 2. Study area

106

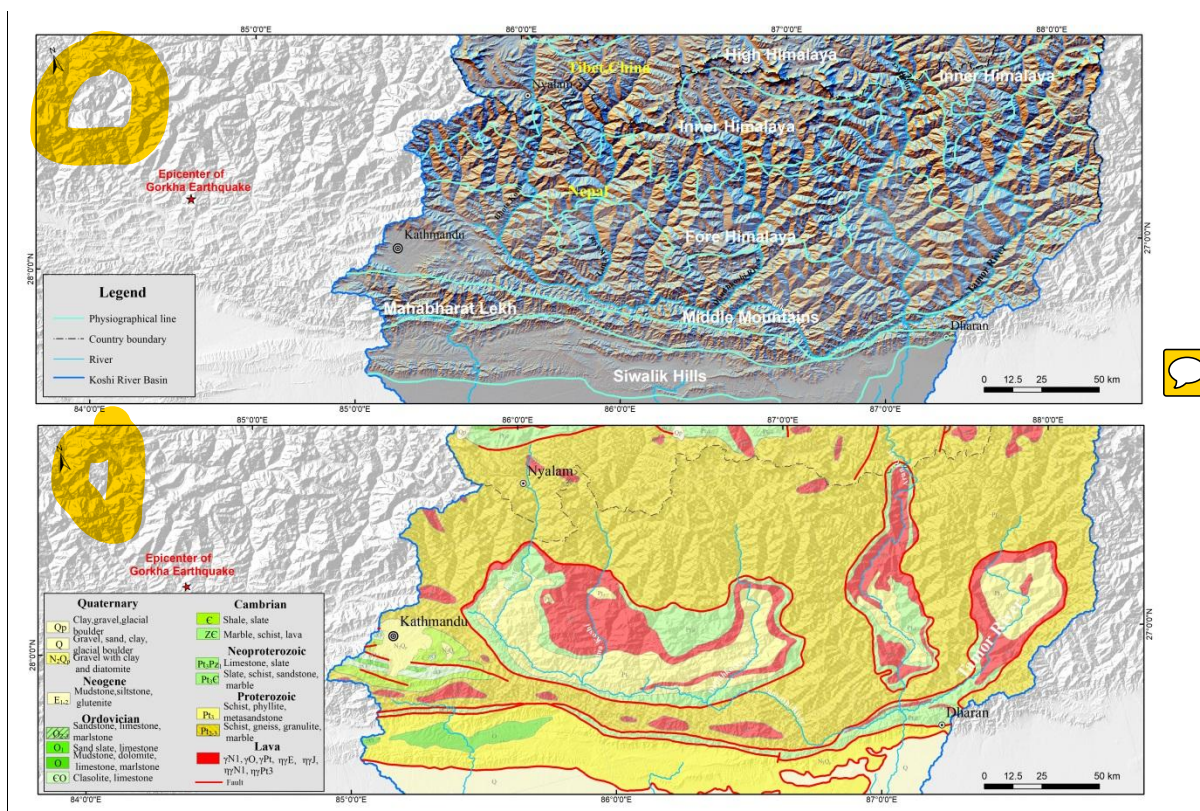
107 The study was carried out in the Koshi River basin, which is a trans-boundary basin located in China, Nepal and India
108 in the central Himalayas (Fig. 1a). The mountainous regions in the upper reaches of the basin where landslides have
109 occurred are located in China and Nepal, and the Indian part consists of relatively flat areas. The elevation of Koshi
110 River basin varies from 60 m a.s.l. at the outlet in India up to 8,844 m at the highest point at Mount Everest. The
111 Koshi basin can be classified into 6 physiographic zones from South to North: Terai, Siwalik Hills, Mahabharat Lekh,
112 Middle Mountains, High Himalaya, and Tibetan Plateau (Gurung and Khanal 1987; Dhital 2015). Considering the
113 distribution of landslides, the Tibetan plateau in the upper reaches and the plains in the lower reaches were excluded.

114 In the Koshi Basin, the major geological structures have an approximate east–west orientation, such as the foreland
115 thrust-fold belt, Main Central Thrust (MCT), South Tibetan Detachment System (STDS) and the Yarlung Zangbo
116 Suture Zone (YZSZ) (Gansser, 1964; Dhital, 2015). The southernmost part of the basin consists of the Quaternary
117 sediments underlain by the Neogene Siwaliks. The Siwaliks comprise soft mudstones, sandstones and conglomerates.
118 In this part of the foreland basin, a number of emergent and blind imbricate faults originate from the Main Himalayan
119 Thrust. The overlying Lesser Himalayan succession forms duplexes and imbricate stacks. The Proterozoic to Miocene
120 rocks of the Lesser Himalaya include limestones, dolomites, slates, phyllites, schists, quartzites, and gneisses (Dhital,
121 2015). A regional-scale thrust MCT separates the Lesser Himalayan sequence from the overlying Higher Himalayan
122 crystallines, which consist of medium- to high-grade metamorphic rocks (e.g., schists, quartzites, amphibolites,
123 marbles, gneisses, and migmatites) and granites aged from the Proterozoic to Miocene. The STDS delineates the
124 Higher Himalayan rocks from the overlying Tethyan sedimentary sequence of Paleozoic–Cenozoic age (Gansser, 1964;
125 Burg et al., 1984; Hodges et al., 1996) (Fig. 1b).

126 In the study area there are three main tributaries of the Koshi River: the Arun (main branch) coming from the north, the
127 Sun Koshi from the west and Tamor from the east. Nearly every year, during the monsoon period, which generally
128 lasts from June to September, the area is affected by rainfall-triggered landslides. Dahal and Hasegawa (2008) used a
129 dataset of 193 landslides occurring from 1951 to 2006, part of which were from the Koshi River basin, to generate a



130 threshold relationship between rainfall intensity, rainfall duration, and landslide initiation.
 131 The area was severely affected by the Gorkha earthquake, with a moment magnitude of 7.8 on 25 April 2015. The
 132 epicenter was located near Gorkha, which is about 80km west of the study area. A second major earthquake occurred
 133 along the same fault on 12 May 2015 with a moment magnitude of 7.3 with the epicenter located inside the Koshi
 134 River basin. The second event is considered as a major aftershock of the main Gorkha earthquake. Both events
 135 triggered many landslides (Collins and Jobson 2015; Kargel et al. 2016; Zhang et al. 2016; Martha et al. 2017).
 136



137
 138 **Fig. 1** Maps showing the study area (a) Physiographic zones of the Koshi River basin; (b) Geological map showing the
 139 main geological zones (Dhital, 2015; Zhang et al. 2016).
 140

141 3. **Input data**

142 The study requires a series of landslide inventory maps, and causal factor maps, which were generated for the middle
 143 part of the Koshi basin, where most of the landslides were concentrated. Two landslide inventories were generated: a
 144 pre-2015 inventory showing rainfall-triggered landslides, and a co-seismic landslide map for the 2015 Gorkha
 145 earthquake. The pre-2015 inventory map was generated using topographic maps, Google Earth and Landsat ETM/TM



146 images. We were able to digitize landslide polygons from the available 1:50,000 scale topographic maps, which cover
147 only the Nepalese part of the Koshi River basin. These maps were generated from aerial photographs acquired in 1992,
148 and landslides were marked as separate units. The smallest landslide with area of 456.6 m² was identified. More recent
149 landslides were mapped from Google Earth images which were captured during Feb. 2015 (Some images were captured
150 in Dec. 2014), using visual image interpretation and screen digitizing. Google Earth supplies high resolution remote
151 sensing imageries from different years, on which even small landslides can be recognized. Landsat ETM imageries and
152 ASTER DEM data were therefore used to adjust the location of the landslides. Landslides with area larger than 50 m²
153 could be recognized by this method. A total of 5,858 rainfall induced landslides were identified in the Koshi River
154 basin.

155 After the 2015 April 25th Gorkha earthquake, it was possible to use images from the Chinese GaoFen-1 and GaoFen-2
156 high resolution satellites of the CNSA (China National Space Administration), which are part of the HDEOS (High-
157 Definition Earth Observation Satellite) program. These images were captured during 27 April, 2015 to May 14 2015.
158 After the earthquake some rainfalls occurred, and the coming monsoon brought more rainfall in earthquake-affected
159 area. **There could be some changes for earthquake-triggered landslide which were impossible to be modified. We tried**
160 **to use the images captured very close to earthquake time in order to reduce the impact by rainfall to landslide after the**
161 **earthquake.** By comparing with images before the earthquake, as well as rainfall-triggered landslide inventory,
162 earthquake-triggered landslides were mapped as polygons, without separating erosion, transportation and accumulation
163 parts, and without a classification in landslide types.

164 For the susceptibility assessment, points located in the source area of landslides, were used as indicative of the
165 initiation conditions.

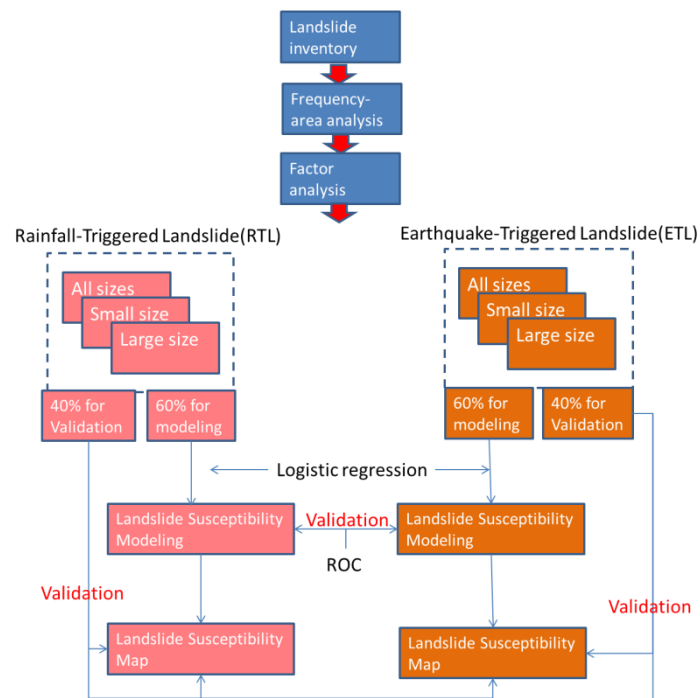
166 The SRTM Digital Elevation Model with **90m spatial resolution** was used in this study. ESRI ArcGIS software enabled
167 the calculation of topographical factors including slope gradient, aspect, curvature, and distance to rivers. The land
168 cover dataset GlobeLand30 with **30×30m spatial resolution**, developed by the National Geomatics Center of China,
169 was employed in this study. The land cover types include cultivated land, forest, grassland, shrub land, wetland, water
170 bodies, tundra, artificial surfaces and bare land. Geological maps of Nepal, and Tibet were obtained from Chengdu
171 Geological Survey Center of the China Geological Survey. The Peak Ground Acceleration data for the Gorkha
172 earthquake were obtained from USGS.

174 4. Methods

175 Figure 2 gives an overview of the method followed in this **study**. The landslide inventories were subdivided into
176 training and test datasets. For each group 60% of the landslide data were used for the modeling, and 40% of the data
177 were used for the validation. Based on the frequency area distribution the RTL and ETL inventories were separated in



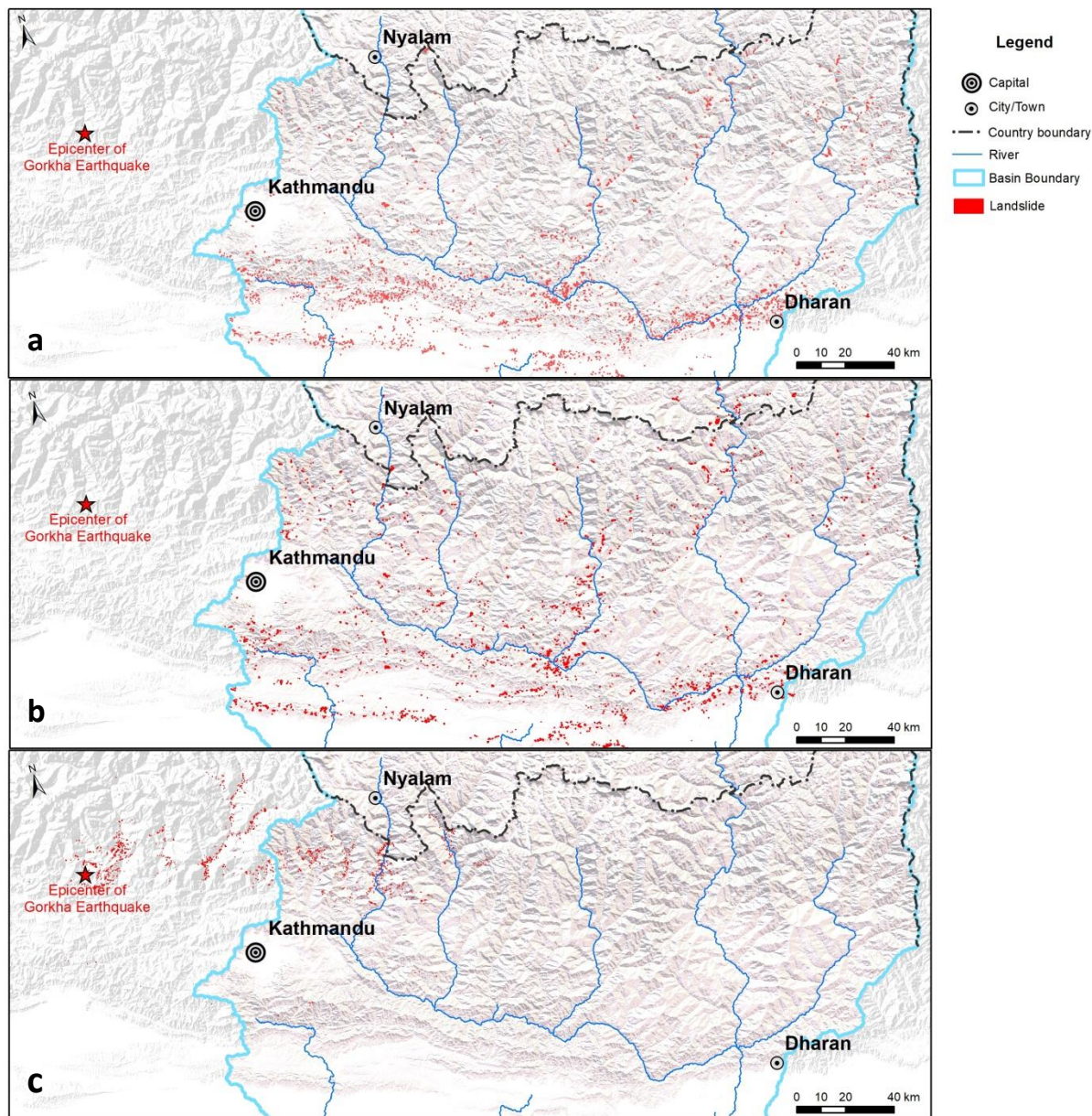
178 two size-groups each. Initially bivariate statistical analysis was used for the different types and sizes of landslides, to
 179 investigate the correlation between landslides and their causal factors. After selecting the relevant factors, the logistic
 180 regression method was used to build the susceptibility model for each size group. The logistic regression method is the
 181 most commonly used model in landslide susceptibility assessment (Ayalew and Yamagishi 2005; Bai et al. 2010; Das et
 182 al. 2010; Nandi and Shakoor 2010; Wang et al. 2013). For the susceptibility modeling of RTL, the following factors
 183 were used: elevation (x_1), slope gradient (x_2), curvature (x_3), slope aspect (x_4), relative relief (x_5), drainage density (x_6),
 184 lithology (x_7), distance to faults (x_8) and land cover type (x_9). For the susceptibility modeling of ETL, peak ground
 185 acceleration (x_{10}) was added. The R software was used to build the models for different types and sizes of landslide
 186 respectively. ROC (Receiver Operating Characteristic) curves were used to verify the accuracy of the susceptibility
 187 models, and finally six landslide susceptibility maps were generated and compared (Fig. 2).



188
 189 **Fig. 2** Methodology for susceptibility assessment to different types and sizes of landslide
 190

191 **5. Landslide characteristics**

192 In the Koshi River basin, a total of 5,858 RTL were mapped. The Gorkha earthquake triggered more than 3000
 193 landslides, of which 1,138 are located in the Koshi River basin. Landslide characteristics were analyzed based on
 194 frequency-area distribution and factor statistics (Fig. 2)



195

196

197

Fig. 3 Landslide inventory of Koshi River basin (a) Landslide inventory of RTL before 1992; (b) Landslide inventory of RTL in 1992~2015; (c) Landslide inventory of ERL by Gorkha earthquake.

198

5.1 Landslide frequency-area distributions

199

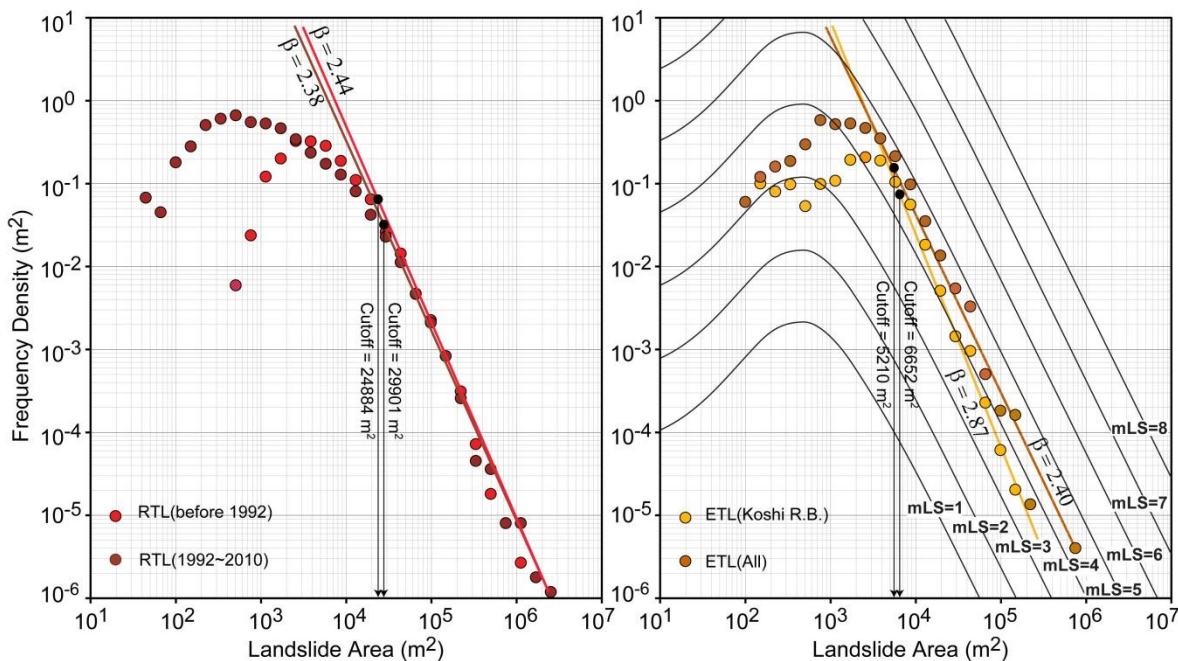
The frequency-area distributions (FAD) of landslides were separately analyzed for both RTL and ETL inventories (Fig.

200

4). For the RTL both landslide inventory data before 1992 and 1992~2015 were analyzed. For the ETL of the Gorkha



201 earthquake, landslides located in the Koshi River basin were analyzed separately from the entire ETL inventory.
 202 Malamud et al. (2004) examined the FAD of landslides and quantified the landslide triggering event with a parameter
 203 called landslide magnitude (mL). In a similar manner, we estimated a mL between 4.0 and 4.5 for the ETL inventory. If
 204 we compare this with the mL of other inventories, we can conclude that this landslide inventory has a landslide
 205 magnitude scale similar to the landslides triggered by the 1994 Northridge event (Harp and Jibson 1995), of 4.0 mL
 206 approximately (Malamud et al. 2004), but lower than the landslide event magnitude of the Wenchuan earthquake which
 207 varies between 4.96 and 6.24, depending on the inventory used (Tanyas et al. 2017). The β value are obtained as
 208 2.44 and 2.38 for the RTL in 1992 and 2010, and 2.40 and 2.87 for all ETL of the Gorkha earthquake and those only
 209 within the Koshi River basin. The cut-off values (which are the landslide areas below which the FAD is no longer
 210 having a powerlaw relation) were 25,000 - 30,000 m² for RTL and 5,000 - 6,600 m² for all ETL.



211
 212 **Fig. 4** Landslide frequency - area analysis in Koshi River basin (a): RTL; (b): ETL.

213
 214 Landslide size classification proposed by Tong (2013) was referenced, where landslides with an area smaller than 1000
 215 m² were classified as small, those with an area between 1,000 m² and 10,000 m² as medium, and those with larger sizes
 216 than 100,000 m² as large size landslides. Based on the results of the FAD analysis, as well as field experience, the RTL
 217 and ETL inventories were subdivided according to landslide size. In order to facilitate the analysis, we subdivided
 218 them into two size-groups, with 6,000 m² boundary value. Landslide data were organized into 6 groups based on



219 the two triggers (rainfall and earthquake) and two size classes (Table 1).

220

221 **Table 1** Numbers for different types and sizes of landslide in Koshi River basin

	Rainfall-triggered landslides (RTL)			Earthquake-triggered landslides (ETL)		
	All sizes	Small size	Large size	All sizes	Small size	Large size
Total	5,858	2,995	2,863	1,138	852	286
Modelling	3,515	1,797	1,718	682	511	171
Validation	2,343	1,198	1,145	456	341	115

222

223 5.2 Correlation of landslides with causal factors

224 Many factor pairs were analyzed using bivariate statistical analysis, and five causative factors that had the highest
225 correlation with landslides were selected for the final analysis: elevation, slope gradient, slope aspect, distance to fault
226 and lithology. The results are summarized in Fig. 5.

227 Statistical analysis was performed for the different size groups of ETL and RTL considering combinations of elevation
228 and slope gradient and the results (Fig. 5a&b) indicate that, RTL are more frequent at lower altitude, especially in the
229 Siwaliks. The numbers of landslide become very small when the altitude higher than 2000 m. ETLs are more frequent
230 in higher elevation, related to the elevation of the blind thrust triggering the earthquake, most of them located in the
231 area with altitude higher than 2000 m. When comparing the size groups it is also clear that small RTLs occur relatively
232 more at lower elevation and less steep slopes than larger RTLs. For ETLs there is no clear differentiation between
233 elevation and slope relations for the two size groups. This may be affected by the types of landslides. Most of the
234 ETLs consist of rockfalls and rockslides which occur in higher and steeper rocky slopes, whereas most RTLs are debris
235 slides located on gentler slopes with soil deposits.

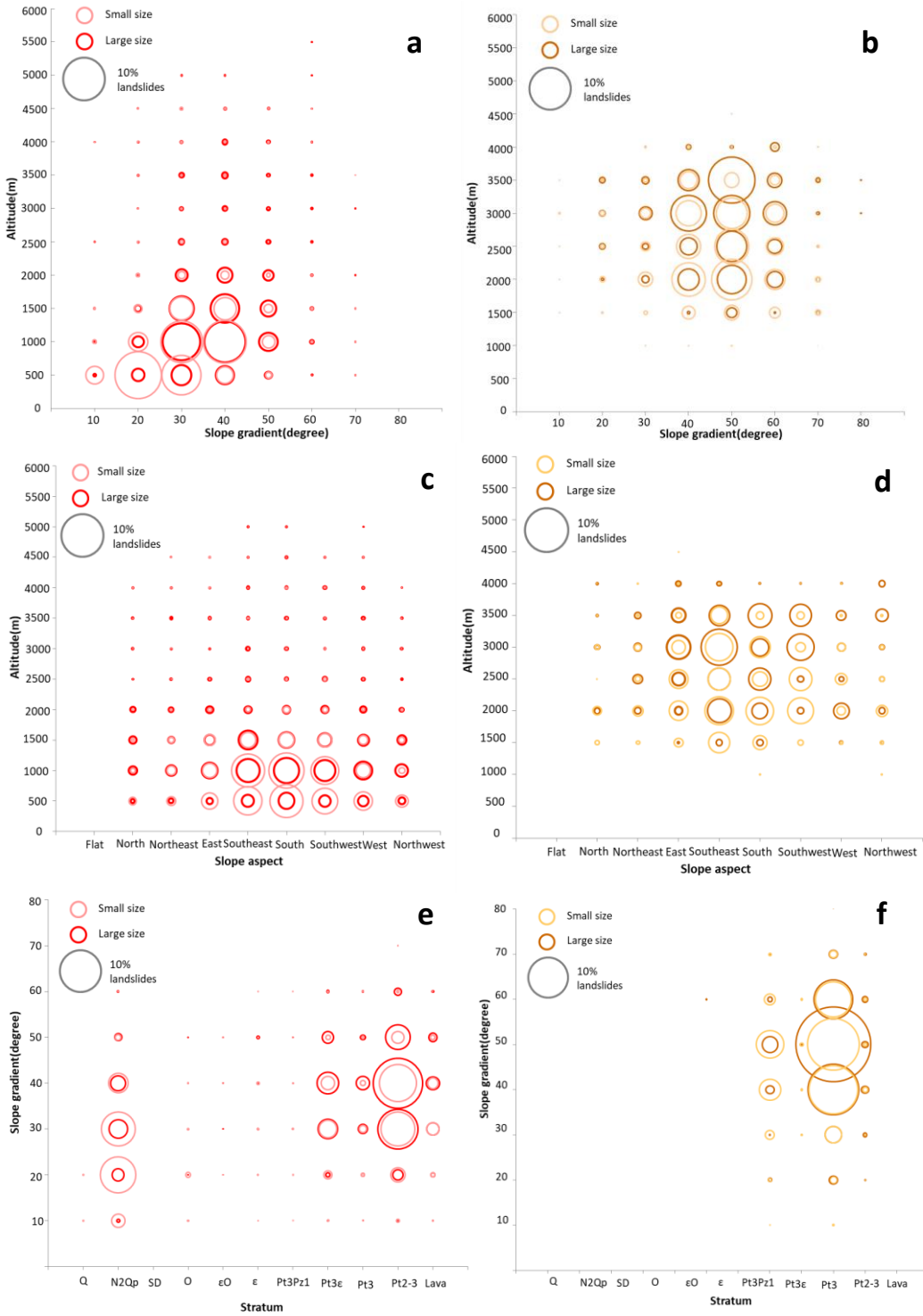


Fig. 5 Correlation between landslides and other factors for rainfall triggered landslides (RTL) on the left side, and

236

237



238 earthquake-triggered landslides (ETL) on the right side. The gray circle shows size for 10% of landslides. a & b:
239 Relation between elevation and slope gradient; c & d: Relation between slope direction and elevation; e & f: Relation
240 between Lithology and slope gradient.

241
242 The slope aspect may have an effect on the occurrence of landslides by influencing the rock weathering, snow melting,
243 and land cover, as well as the transmission of seismic waves (Kamp et al. 2008). Fig. 5 c&d show the correlation
244 between landslides, altitude and slope aspect. The majority of RTLs is located on slopes directed to the . In different
245 altitude, RTLs show the same relationship with slope aspect. These slope aspects are windward slope with more
246 precipitations, which supply the trigger for landslides. Most of ETLs are also distributed in south, southeast or
247 southwest slopes, but with increasing of altitude, the relationship with slope aspect changes. The comparison of the size
248 groups showed that, most large size ETLs are located on south and southwest facing slopes with high elevation, while
249 more small-size ETLs are located in similar slope directions but in relatively lower elevations (Fig. 5 c&d).

250 Fig. 5e&f show the relation with slope and lithology. RTLs are concentrated on Proterozoic metamorphic lithological
251 units (Pt₂₋₃), consisting of schist, gneiss, and marble and in Quaternary molasse (N₂Qp) units (See Fig. 1). The Pt₂₋₃
252 unit contains landslides of both size classes located in the steeper slopes with gradient of 20°-40°, while in the unit
253 N₂Qp, more landslides are located in gentler slopes with gradient 10°-30°. The statistics also showed that, in the unit of
254 N₂Qp with weaker rocks there were more small size landslides, and in the unit of Pt₂₋₃ with stronger rocks there are
255 more large size landslides.

256 ETLs also concentrated on Pt₂₋₃, but more ETL are located in steeper slopes. The percentages for large size and small
257 size of ETL are similar in different slope interval except in slopes of 40° -50°, where more large size landslides have
258 occurred.

259
260

261 **6. Landslide susceptibility assessment**

262 6.1 Landslide susceptibility models

263 For the susceptibility modeling of RTL, the contributing factors include: elevation(x₁), slope gradient(x₂),
264 curvature(x₃), slope aspect(x₄), relative relief(x₅), gully density(x₆), lithology(x₇), distance to fault(x₈) and land cover
265 type(x₉). The Peak Ground Acceleration, PGA, (x₁₀) was added to the assessing factors for the susceptibility modeling
266 of ETL. The R software was used to build the models for different types and sizes of landslides respectively (Table 2).
267 Weight of landslide susceptibility models show differences between different triggers and different sizes of landslides.
268 Altitude, curvature and slope gradient with weights of -7.5456, -6.2341 and 6.1481 respectively have high impact on
269 susceptibility of RTL, while relative relief, curvature and slope gradient with weights of 24.4495, -22.4360 and 8.7348



270 have high impact on susceptibility of ETL. Factors of curvature and relative relief show differences for small size and
 271 large size of RTL; elevation and curvature were very different between small size and large size of ETL.

272

273

Table 2 Susceptibility models for different triggers and sizes of landslide in Koshi River basin

Landslide type	x_1	x_2	x_3	x_4	x_5	x_6	x_7	x_8	x_9	x_{10}	p	AUC
All RTL	-7.5457	6.1481	-6.2341	-0.1131	-2.3020	-0.6447	1.3392	-0.4253	1.1421	-	2.8968	0.820
Small size RTL	-9.5260	6.1132	-12.0070	-0.2230	-6.1225	-2.0765	1.4518	-0.9228	-0.9673	-	9.4669	0.809
Large size RTL	-7.16699	6.20998	-5.12041	0.10008	2.13507	-0.23847	0.95660	-0.01205	1.58680	-	1.21971	0.852
All ETL	-1.5853	8.7368	-22.4360	-0.1432	24.4495	5.9713	2.4447	0.2831	0.9352	5.5455	5.9066	0.940
Small size ETL	-0.85231	8.07288	-32.9325	0.06238	23.9783	5.31668	2.46812	0.34372	1.15004	5.66908	13.3380	0.941
Large size ETL	-4.0451	8.3146	-11.9824	0.3314	25.3506	3.5029	2.7321	-0.4193	-0.7274	6.5423	-1.0992	0.940

274

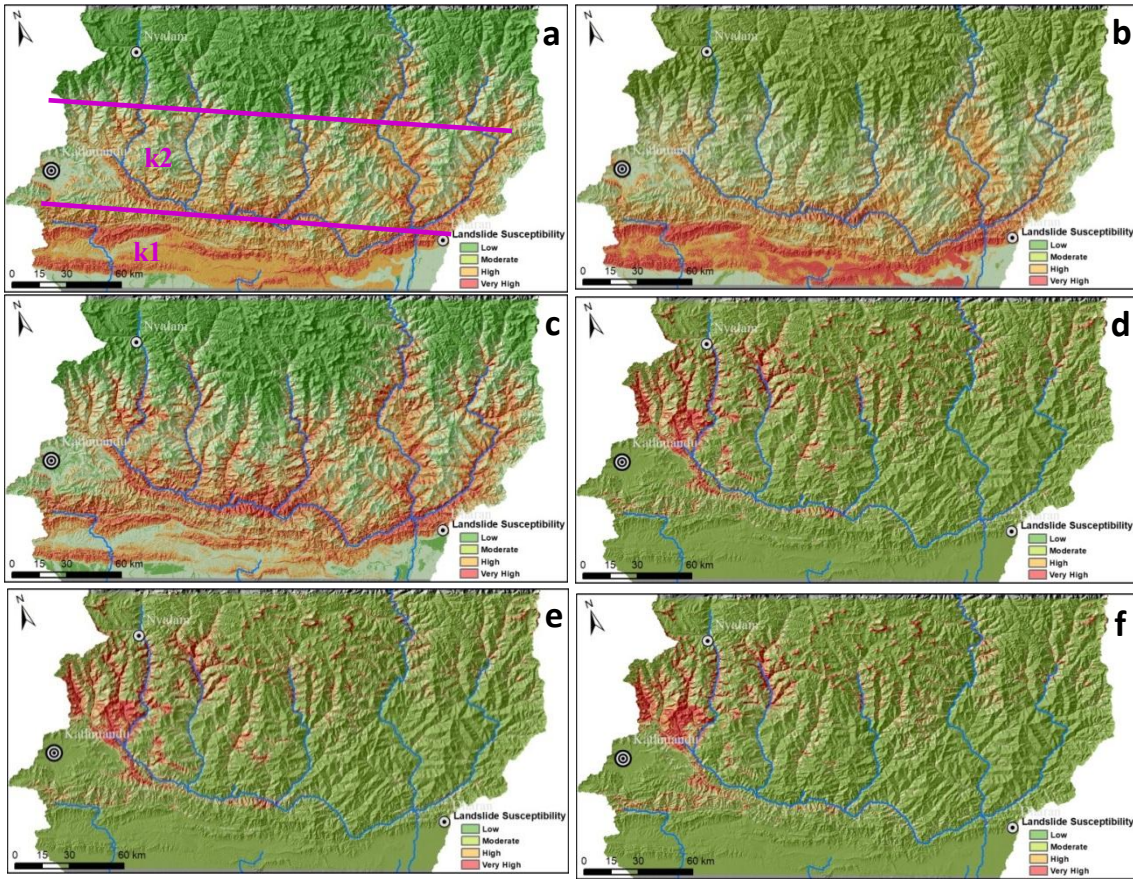
275 6.2 Result

276 The logistic regression models were applied to the Koshi River basin, and in total six susceptibility maps were
 277 generated (Fig. 6). Susceptibility values were classified into four levels: low, moderate, high and very high, based on
 278 the following susceptibility threshold values: 0-0.25, 0.25-0.5, 0.5-0.75 and 0.75-1.

279 The RTL susceptibility map (Fig. 6a) shows that high and very high susceptible are located mostly in the Siwaliks and
 280 in the Mahabharat Lekh region in west-eastern direction and the Middle to High Himalaya region in north-south
 281 direction. The Siwaliks and Mahabharat Lekh regions have high and very high susceptibility levels for small
 282 landslides, and lower susceptibility levels for large ones. The Middle and High Himalaya region has a reverse
 283 situation: high and very high susceptibility levels for large landslides, and lower levels for small ones.

284 The ETL susceptibility map reflects the co-seismic landslide pattern of the Gorkha earthquake, with very high and high
 285 susceptibility in the western part of the Koshi. It is important to note that the ETL susceptibility map only reflects the
 286 characteristics of the Gorkha earthquake and is therefore not a reliable map for future earthquakes that may have
 287 another epicentral location, length of fault ruptures and magnitudes.

288 There is no much difference between susceptibility maps for small size ETL and large size ETL. First hand, this may
 289 be due to the far distance to the earthquake epicenter. The earthquake has low impact to the large size ETL. From the
 290 study on ETL by the 2008 Wenchuan earthquake, the study showed that 80% of large size landslide concentrated in the
 291 distance less than 5 km to the main faults (Xu and Li 2010). Second hand the large size ETL may relate to other factors
 292 including secondary faults, rock structure, which need more detail information.



293

294

295

296

297

298

299

300

301

302

303

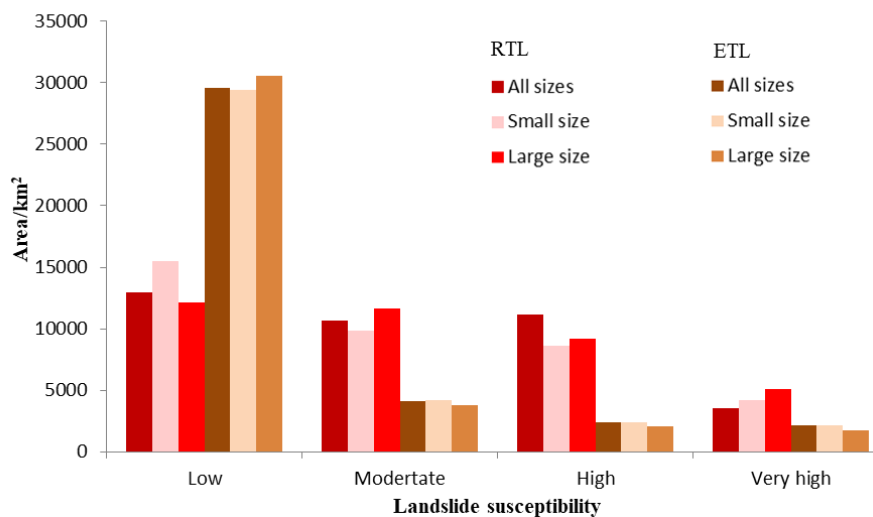
304

Fig. 6 Susceptibility maps for different sizes of RTL and ETL: (a) for all RTLs; (b) for small RTLs; (c) for large RTLs; (d) for all ETLs; (e) for small ETLs; (f) for large ETLs.

The areal coverage of the different levels of landslide susceptibility was calculated for each susceptibility map (Fig. 7). Compared to RTL, the ETL susceptibility maps have a larger area with low susceptibility, due to fact that the Koshi River basin is far from the epicenter of Gorkha earthquake, thus the earthquake affected region is not large. The very high and high susceptible region for ETL is mostly concentrated in the southern part of the basin. Thus it can be concluded that rainfall has a wider and stronger effect on landslide occurrence than the Gorkha earthquake in Koshi River basin.

The very high and high susceptibility areas for large size ETLs is larger than small size ETLs, while the very high and high susceptible area for large size RTL is smaller than small size RTL.





305
306 **Fig. 7** Statistics of areas for different landslide susceptibility levels on the susceptibility maps
307

308 ROC curves were drawn to verify the accuracy of each susceptibility model (Fig. 8), and the Area Under Curve
309 (AUC) was calculated (See Table 2). The AUC values of the ETL models were higher than for RTL, since the ETL
310 were more concentrated than the RTL, as the inventory is from one single triggering event, whereas the RTLs are from
311 many different rainfall events over a longer time period.

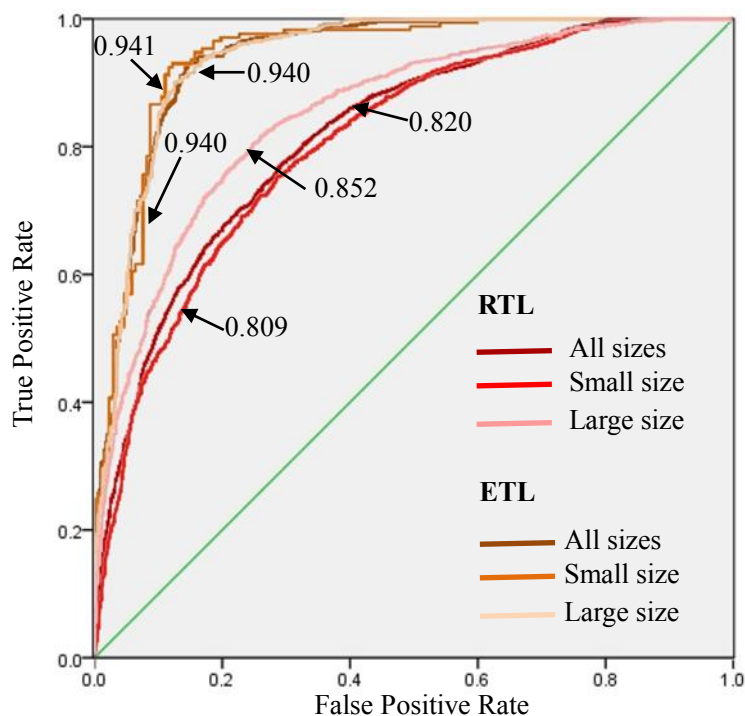


Fig. 8 ROC curves for the susceptibility assessing models to different sizes of RTL and ETL

7. Cross-validation of landslide susceptibility maps

Different groups of landslide data were used to validate the landslide susceptibility maps for RTL and ETL. For each trigger and sizeclass, the number of landslides was calculated, inside the areas with a certain susceptibility level, to cross-validate the results.



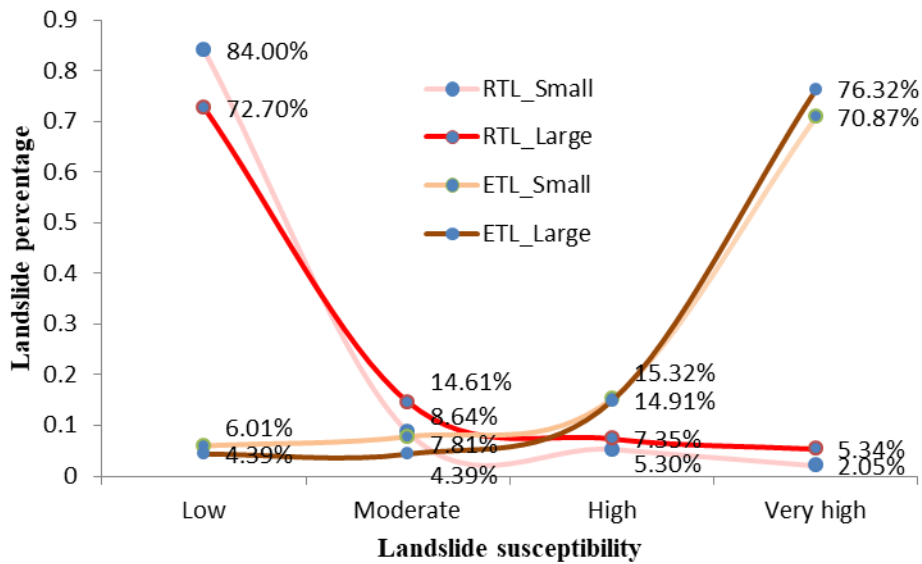
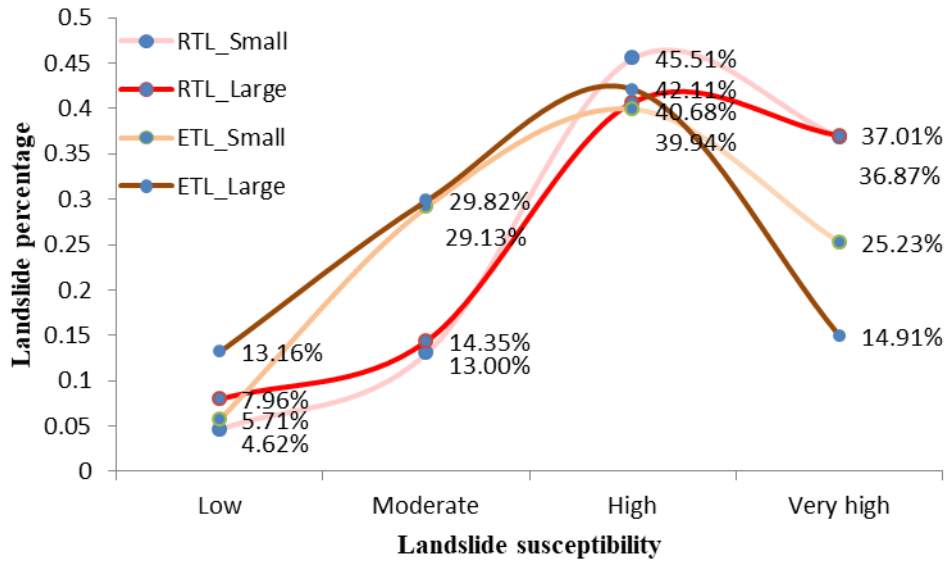




Fig. 9 Cross validation of the landslide susceptibility maps. (a) The percentage of landslides in the various classes of the RTL susceptibility map. (b) The percentage of landslides in the various classes of the ETL susceptibility map.

The percentages of different size RTLs and ETLs in each susceptibility are shown in Fig. 9. For the RTL susceptibility map, percentages of small size and large size landslides show a similar tendency, for both triggers. More than 40 percent of the landslides were located in high susceptibility zones. There is a marked difference between the percentages of ETL and RTL in the ETL landslide susceptibility classes. The RTL are generally much better predicted



329 than the ETL, of which about 29 % occurs in the moderate class. There is a significant difference in the percentage of
330 landslide sizes for ETL in the low and high susceptibility classes. For ETL there is a difference in the low and very
331 high classes.

332 For the ETL susceptibility map  RTL and ETL percentages show completely different patterns. Most of the RTLs
333 (both small and large) are located in the low ETL susceptible regions. Conversely, a large fraction of small size and
334 large size of ETLs are located in the high susceptible regions. **The conclusion that can be drawn is that the regions with
335 very high and high susceptibility to ETL are not prone to RTL. This might change however, in the coming period, as the
336 earthquake triggered landslides are bare and often the source of loose debris, that can be reactivated by extreme rainfall
337 events.** 

338 8. Discussion and conclusions

339 This study aimed to analyze independent rainfall- (RTL) and earthquake-triggered landslide (ETL) inventories for a
340 large mountainous watershed in the Himalayas, located in India, Nepal and China. Based on the results of the FAD
341 analysis, the RTL and ETL inventories were subdivided according to landslide size, with a threshold value of 6000 m².
342 The distribution of RTL shows high correlation with altitude and slope aspect due to precipitation. Most of the pre-
343 2015 RTLs are located below 2000 m, and these landslides are more concentrated on south oriented slopes. As the
344 moist airflow from the India Ocean continues to pass over the main crest of the Himalayas, it brings lots of
345 precipitation with increase of altitude, especially on the windward slopes including south, southeast and south west.
346 The high precipitation triggers lots of landslides in these slopes. The airflow loses much of its moisture and warms up
347 as it descends. The rain shadow is formed in the north slopes of the Himalayas, where precipitation rate becomes very
348 low (Zurick and Pacheco 2006). ETL also show different correlation with elevation and aspect. It is more due to the
349 location of epicenter and the propagation direction of seismic wave.

350 Combination of slope gradient with altitude and lithology affect the size of RTL strongly. There was a clear correlation
351 between the size of the landslides, the slope gradient and altitude. Small RTLs occurred more at lower elevations and
352 less steep slopes relatively, while most large size RTLs are located in higher elevation with steeper slopes. There is no
353 clear differentiation between elevation and slope relations for the two size groups of ETL except in the region with
354 3500m elevation and 50° slope gradient. ETLs occur more frequently on steeper slopes and in metamorphic rocks than
355 RTLs, which are more prominent in weak sedimentary rocks and colluvium materials.

356 Weight of landslide susceptibility models can also indicate the significance of causal factors. Altitude, curvature and
357 slope gradient with weights of -7.5456, -6.2341 and 6.1481 respectively have high impact on susceptibility of RTL,
358 while relative relief, curvature and slope gradient with weights of 24.4495, -22.4360 and 8.7348 have high impact on
359 susceptibility of ETL. For different size of RTL and ETL, curvature shows significant difference between small size and
360 large size.



361 The correlation between causal factors and landslide inventories resulted in very different maps for earthquake and
362 rainfall triggered landslides. Most susceptible areas to RTL are located in the Siwalik and Mahabharat Lekh area, with
363 structures oriented in west-east direction, and in the river valleys in the Middle Mountains which are mostly oriented in
364 a north-south direction. ETLs are most likely in the western part of the basin, which is related to the fact that the
365 Gorkha earthquake occurred to the west of the Koshi River basin. The susceptible areas to ETL are much smaller than
366 RTL, and most of them are located on the north, in altitudes between 2000 and 3500 m. The susceptibility map for
367 small size ETL is very similar to the susceptibility map for large size ETL due to the far distance to earthquake
368 epicenter. Some more detail information could be included in large scale research.

369 The cross-validation showed that the RTL susceptibility map has a modest capability of explaining the ETL pattern,
370 but that the ETL susceptibility cannot properly predict the RTLs. Although landslide size matters, especially for RTLs,
371 there is not such a large difference in behavior for the ETLs. This means one should be careful with using
372 susceptibility maps that were made for earthquake induced landslides, as prediction tools for rainfall induced
373 landslides. Such maps are in fact of little practical implication, as the next earthquake may not be likely to occur in the
374 same location and therefore produce a similar landslide pattern. More advanced methods are required in order to derive
375 earthquake-triggered landslide susceptibility maps, making use of physically-based modelling for many possible
376 earthquake scenarios. Whereas, the use of rainfall-triggered landslide maps can be of some use for predicting the
377 occurrence of earthquake-triggered landslides, one should be careful, as the specific location of the earthquake plays a
378 dominant role. Landslide susceptibility map should also be updated after major earthquakes, as the presence of bare
379 areas with loose debris might trigger more rainfall induced landslides in the years following the earthquake. A major
380 limitation in this work was that we were not able to use separate event-based inventories for RTLs, and only one event-
381 based inventory for ETL. The collection of event-based inventories, both for rainfall and earthquake triggers, remains
382 one of the main challenges in order to advance the study of landslide hazard at a watershed scale.

383 The Gorkha earthquake triggered a large number of landslides in this basin. Meanwhile the earthquake affected the
384 structure and stability of slopes strongly. So after the earthquake, landslides become more active under the impact of
385 rainfall. What are the characteristics of RTL after earthquake and ETL? Weather there is difference between RTL
386 before earthquake and RTL after earthquake? These could be the further study.

387

388 **9. Acknowledgements**

389 This research was supported by the National Natural Science Foundation of China (Grant No.41401007), the External
390 Cooperation Program of BIC, Chinese Academy of Sciences (Grant No. 131551KYSB20130003). This study was also
391 jointly supported by the Australian government funded Koshi Basin Programme at ICIMOD as well as ICIMOD's core
392 funds contributed by the governments of Afghanistan, Australia, Austria, Bangladesh, Bhutan, China, India, Myanmar,



393 Nepal, Norway, Pakistan, Switzerland, and the United Kingdom.

394

395

396 **References**

397 Ayalew L, Yamagishi H (2005) The application of GIS-based logistic regression for landslide susceptibility mapping in
398 the Kakuda-Yahiko Mountains, Central Japan. *Geomorphology* 65(1–2): 15–31,
399 doi:10.1016/j.geomorph.2004.06.010

400 Bathrellos GD, Kalivas D and Skilodimou HD (2009) GIS-based landslide susceptibility mapping models applied to
401 natural and urban planning in Trikala, Central Greece. *Estud Geol* 65(1): 49–65. doi: 10.3989/egeol.08642.036

402 Bai S, Wang J, Lü GN, Zhou PG, Hou SS and Xu SN (2010) GIS-based logistic regression for landslide susceptibility
403 mapping of the Zhongxian segment in the Three Gorges area, China. *Geomorphology* 115(1–2): 23–31.
404 doi:10.1016/j.geomorph.2009.09.025

405 Burg JP, Guiraud M, Chen GM, Li GC (1984) Himalayan metamorphism and deformations in the North Himalayan
406 Belt (southern Tibet, China), *Earth Planet Sci Lett*, 69:391–400.

407 Carrara A, Cardinali M, Guzzetti F, and Reichenbach P (1995) GIS technology in mapping landslide hazard, In:
408 Carrara A and Guzzetti F (eds), *Geographical Information Systems in Assessing Natural Hazards*, Kluwer
409 Academic Publishers, Dordrecht, The Netherlands

410 Chang KT, Chiang SH and Hsu ML (2007) Modeling typhoon- and earthquake-induced landslides in a mountainous
411 watershed using logistic regression. *Geomorphology* 89(3–4): 335–347. doi:10.1016/j.geomorph.2006.12.011

412 Chung CJF, Fabbri AG (1993) The representation of geoscience information for data integration. *Nonrenewable
413 Resources* 2(2): 122–139. doi: 10.1007/BF02272809

414 Collins BD, Jibson RW (2015) Assessment of existing and potential landslide hazards resulting from the April 25,
415 2015 Gorkha, Nepal earthquake sequence, U.S. Geological Survey OpenFile Report 2015-1142, Reston, VA

416 Dai FC, Lee CF (2001) Frequency-volume relation and prediction of rainfall-induced landslides. *Engineering Geology*
417 59(3–4): 253–266. doi:10.1016/S0013-7952(00)00077-6

418 Dahal RK, Hasegawa S (2008) Representative rainfall thresholds for landslides in the Nepal Himalaya.
419 *Geomorphology* 100 (3–4): 429–443. doi:10.1016/j.geomorph.2008.01.014

420 Das I, Sahoo S, van Westen CJ, Stain A, Hack R (2000) Landslide susceptibility assessment using logistic regression
421 and its comparison with a rock mass classification system, along a road section in the northern Himalayas
422 (India). *Geomorphology* 114(4): 627–637, doi:10.1016/j.geomorph.2009.09.023

423 Dhital MR (2015) *Geology of the Nepal Himalaya, Regional Perspective of the Classic Collided Orogen*, Springer,



- 424 Switzerland. doi:10.1007/978-3-319-02496-7
- 425 Dilley M, Chen RS, Deichmann U, Lerner-Lam AL, Arnold M (2005) Natural disaster hotspots: a global risk analysis,
426 The World Bank Hazard Management Unit, Washington
- 427 Duman TY, Can T, Gokceoglu C, Nefeslioglu HA, Sonmez H (2006) Application of logistic regression for landslide
428 susceptibility zoning of Cekmece Area, Istanbul, Turkey. *Environmental Geology* 51(2): 241-256.
429 doi:10.1007/s00254-006-0322-1
- 430 Elliott JR, Jolivet R, González PJ, Avouac J-P, Hollingsworth J, Searle MP, Stevens VL (2016) Himalayan megathrust
431 geometry and relation to topography revealed by the Gorkha earthquake. *Nature Geoscience* 9:174–180.
432 doi:10.1038/ngeo2623
- 433 Gansser A (1964) *Geology of the Himalayas*, Interscience, New York
- 434 Gurung HB and Khanal NR (1987) *Landscape processes in the Chure range*, Nepal National Committee for Man and
435 the Biosphere, Kathmandu
- 436 Guzzetti F, Carrara A, Cardinali M, Reichenbach P (1999) Landslide hazard evaluation: a review of current techniques
437 and their application in a multi-scale study, Central Italy. *Geomorphology* 31: 181-216, doi:10.1016/S0169-
438 555X(99)00078-1
- 439 Guzzetti F, Ardizzone F, Cardinali M, Rossi M, Valigi D (2008) Landslide volumes and landslide mobilization rates in
440 Umbria, central Italy. *Earth and Planetary Science Letters* 279(3-4): 222-229. doi:10.1016/j.epsl.2009.01.005
- 441 Haque U, Blum P, da Silva PF, Andersen P, Pilz J, Chalov SR, Malet J-P, Auflič MJ, Andres N, Royiadji E, Lamas PC,
442 Zhang W, Peshevski I (2016) Fatal landslides in Europe. *Landslides* 13(6): 1545–1554. doi:10.1007/s10346-
443 016-0689-3
- 444 Harp EL, Jibson RW (1996) Landslides triggered by the 1994 Northridge, California earthquake. *Bulletin of the*
445 *Seismological Society of America* 86: S319-S332
- 446 Hodges KV, Parrish RR, Searle MP (1996) Tectonic evolution of the central Annapurna Range, Nepalese Himalaya,
447 *Tectonics*, 15:1264–1291
- 448 Kamp U, Growley BJ, Khattak GA, Owen LA (2008) GIS-based landslide susceptibility mapping for the 2005
449 Kashmir earthquake region. *Geomorphology* 101: 631-642. doi: 10.1016/j.geomorph.2008.03.003
- 450 Kargel J, Leonard G, Shugar D. et al. (2016) Geomorphic and geologic controls of geohazards induced by Nepal's
451 2015 Gorkha earthquake. *Science* 351(6269), aac8353. doi:10.1126/science.aac8353
- 452 Klar A, Aharonow E, Kalderon-Asael B, Katz O (2011) Analytical and observational relations between landslide
453 volume and surface area. *Journal of Geophysical Research* 116(F2): 1-10. doi:10.1029/2009JF001604
- 454 Korup, O., Clague, J.J., Hermanns, R.L., Hewitt, K., Strom, A.L., Weidinger, J.T. (2007) . Giant landslides
455 topography and erosion. *Earth Planet. Sci. Lett.* 261, 578 - 589.



- 456 Larsen IJ, Montgomery DR (2012) Landslide erosion coupled to tectonics and river incision. *Nature Geoscience* 5(7),
457 468–473. doi:10.1038/ngeo1479
- 458 Larsen IJ, Montgomery DR, Korup O (2011) Landslide erosion controlled by hillslope material. *Nature Geoscience*
459 3(4), 247-251. doi:10.1038/ngeo776
- 460 Peng L, Xu S, Peng J (2014). Research on development characteristics and size of landslide in the Three Gorges area.
461 *Geoscience*. 28(5): 1077-1086.
- 462 Lin CW, Liu SH, Lee SY, Liu CC (2006) Impacts of the Chi-Chi earthquake on subsequent rainfall-induced landslides
463 in central Taiwan. *Engineering Geology* 86(2-3): 87–101. doi:10.1016/j.enggeo.2006.02.010
- 464 Malamud BD, Turcotte DL, Guzzetti F, Reichenbach P (2004) Landslide inventories and their statistical properties.
465 *Earth Surf. Process. Landform* 29:687-711. doi:10.1002/esp.1064
- 466 Martha TR, Reddy PS, Bhatt CM, Govindha Raj KB, Nalini J, Padmanabha A, Narender B, Kumar KV,
467 Muralikrishnan S, Rao GS, Diwakar PG, Dadhwal VK(2017) Debris volume estimation and monitoring of
468 Phuktal river landslide-dammed lake in the Zaskar Himalayas, India using Cartosat-2 images. *Landslides*
469 14(1): 373-383. doi: 10.1007/s10346-016-0749-8
- 470 Martha TR, Roy P, Mazumdar R, Govindharaj KB, Kumar KV(2017) Spatial characteristics of landslides triggered by
471 the 2015 Mw 7.8 (Gorkha) and Mw 7.3 (Dolakha) earthquakes in Nepal. *Landslides* 14(2): 697–704.
472 doi:10.1007/s10346-016-0763-x
- 473 Menuier P, Hovius N and Haines JA (2008) Topographic site effects and the location of earthquake induced landslides.
474 *Earth and Planetary Science Letters* 275(3-4): 221-232. doi:10.1016/j.epsl.2008.07.020
- 475 Nandi A, Shakoor A(2010) A GIS-based landslide susceptibility evaluation using bivariate and multivariate statistical
476 analyses. *Engineering Geology* 110(1–2): 11-20. doi:10.1016/j.enggeo.2009.10.001
- 477 Petley D (2012) Global patterns of loss of life from landslides. *Geology* 40(10): 927–930. doi:10.1130/G33217.1
- 478 SafeLand (2015) Guidelines for landslide susceptibility, hazard and risk assessment and zoning,
479 <https://www.ngi.no/eng/Projects/SafeLand>
- 480 Soeters R, van Westen CJ (1996) Slope instability recognition, analysis, and zonation. In: Turner AK, Schuster
481 RL(eds), *Landslides, investigation and mitigation*, Washington D.C., National Academy Press
- 482 Tang C, Zhu J, Qi X (2010) Landslide hazard assessment of the 2008 Wenchuan earthquake: a case study in Beichuan
483 area. *Canadian Geotechnical Journal* 48(1): 128-145. doi:10.1139/T10-059
- 484 Tang C, van Westen CJ, Tanyas H, Jetten VG (2016) Analysing post-earthquake landslide activity using multi-
485 temporal landslide inventories near the epicentral area of the 2008 Wenchuan earthquake. *Nat. Hazards Earth*
486 *Syst. Sci.* 16: 2641-2655. doi:10.5194/nhess-16-2641-2016
- 487 Tanyas H, van Westen CJ, Allstadt KE(2017) New method for estimation of landslide-event magnitude based on large



- 488 dataset of earthquake-induced landslides. *Earth Surface Processes and Landforms* (Accept)
- 489 Tong L, Qi S, An G, Liu C (2013) Large scale geo-hazards investigation by remote sensing in Himalayan region,
490 Science Press, Beijing (in Chinese)
- 491 van Westen CJ, Castellanos E, Kuriakose SL (2008) Spatial data for landslide susceptibility, hazard, and vulnerability
492 assessment: An overview. *Eng Geol* 102(3-4): 112–131. doi:10.1016/j.enggeo.2008.03.010
- 493 Wang L, Sawada K, Moriguchi S (2013) Landslide susceptibility analysis with logistic regression model based on
494 FCM sampling strategy. *Computers & Geosciences* 57: 81-92. doi:10.1016/j.cageo.2013.04.006
- 495 Xu Q and Li W (2010) Distribution of large-scale landslides induced by the Wenchuan earthquake. *Journal of*
496 *Engineering Geology* 18(6) : 818-826(in Chinese)
- 497 Zhang J, Gurung DR, Liu RK, Murthy MSR, Su FH (2015) Abe Berek landslide and landslide susceptibility assessment
498 in Badakhshan Province, Afghanistan. *Landslides* 12(3): 597-609. doi: 10.1007/s10346-015-0558-5
- 499 Zhang J, Liu R, Deng W, Khanal NR, Gurung DR, Murthy MSR, Wahid S(2016) Characteristics of landslide in Koshi
500 River basin, central Himalaya. *Journal of Mountain Science* 13(10):1711-1722. doi :10.1007/s11629-016-4017-
501 0
- 502 Zurick D and Pacheco J (2006) *Illustrated atlas of the Himalaya*. New Delhi, University Press of Kentucky Lexington
503 and India Research Press
- 504